

Depth-dependent earthquake focal mechanism orientation: Evidence for a weak zone in the lower crust

Götz H. R. Bokelmann and Gregory C. Beroza

Department of Geophysics, Stanford University, Stanford, California

Abstract. The traction free boundary condition across the Earth's surface provides an opportunity for studying the relationship between stress orientation and earthquake focal mechanisms because it requires alignment of principal stress axes with vertical and horizontal orientations. A survey of earthquake focal mechanisms in northern California shows that their principal axes are also closely aligned with the vertical and the horizontal in the upper few kilometers of Earth's crust. Thus the signature of the free surface boundary condition on stress appears in focal mechanism orientations as well. The focal mechanism alignment can also be characterized by the relative magnitude of the off-diagonal elements, M_{xz} and M_{yz} , of the seismic moment tensor. We find significant and systematic depth variations in the "horizontal moment tensor element" m_s , which relates to the shear traction acting on a horizontal plane for the special case of perfect alignment between principal stress and focal mechanism axes. Values of m_s near Earth's surface are small but increase with depth to a maximum between 5 and 8 km. At greater depths, there is a gradual decrease, which suggests decreasing horizontal shear traction toward the base of the seismogenic zone. We interpret this tendency of axes to become oriented near the base of the seismogenic zone (and its expression in m_s) as the signature of a weak zone in the lower crust. If correct, this observation would have important implications for the mechanics of lithospheric deformation.

1. Introduction

The nature of crustal deformation depends strongly on the variation of rheological properties with depth; however, the rheology of the lower crust and its relation to the underlying mantle is poorly constrained. There have been suggestions for both a relatively weak and a relatively strong lower crust. *Lachenbruch and Sass* [1973] and *Thatcher and England* [1998] invoke a strong lower crust to explain the broad zone of high heat flow across the San Andreas fault system and to maintain force equilibrium in the presence of weak fault zones. Other studies suggest that the lower crust is mechanically weak compared to the upper crust, since the lower crust deforms by plastic deformation instead of brittle failure [*Scholz*, 1988]. Geological observations in regions of normal faulting [*Jackson and McKenzie*, 1983], lack of Moho offsets in other regions [*Froidevaux*, 1986; *Zuber et al.*, 1986], and laminated reflectivity patterns [*Fuchs et al.*, 1987] are all suggestive of a weak zone in the lower crust. There is, however, little if any direct quantitative evidence [*Molnar*, 1992].

It is important to understand the behavior of the lower crust, since it has considerable influence on the style of crustal deformation, the nature of large earthquake recurrence, and more generally, the long-term evolution of the crust and mantle. If the lower crust is weak, the upper crust and mantle may be partly decoupled over local and regional length scales [*Royden*, 1996]. If, on the other hand, mantle and crust are mechanically coupled [*England and Jackson*, 1989], then they deform coherently and crustal deformation may directly reflect deformation in the mantle [*Silver*, 1996]. The depth variation of stress, if it could be measured, would also place important constraints on the depth variation of mechanical properties of the crust.

Of the indicators used to infer the state of stress, earthquake focal mechanism orientations provide the most comprehensive and widespread stress information [*Zoback and Zoback*, 1980]. They also offer the considerable advantage of sampling the stress field at depth rather than near the surface. In general, the relationship between stress and faulting is not simple. As shown by *McKenzie* [1969], the hypothesis that slip occurs in the direction of resolved shear traction across the fault plane only restricts the direction of maximum compressive stress to lie within the dilational quadrant of the fault plane solution. On the basis of this understanding, a number of techniques have been developed to

Copyright 2000 by the American Geophysical Union.

Paper number 2000JB900205.
0148-0227/00/2000JB900205\$09.00

infer stress conditions from focal mechanism data [e.g., *Gephart and Forsyth, 1984*]. Frictional considerations limit the range of allowable stress states further, but they may be problematic to apply since we may be dealing with faults of differing frictional strength. In particular, there is evidence that faults may be weak such that they slip at very low levels of friction [*Lachenbruch and Sass, 1973; Zoback et al., 1987; Iio, 1997*].

In this study we take a different approach. Rather than try to infer the state of stress from focal mechanism data, we use the free surface boundary condition to orient the principal stress axes. Since there is no traction acting across Earth's surface, the stress components σ_{xz} , σ_{yz} , and σ_{zz} must all vanish. This causes one of the principal stress directions to be vertical and the other two to be horizontal. We examine the orientation of focal mechanisms of the shallowest earthquakes and find that they follow the expected orientation for the stress axes. That is, one of the principal axes of the fault plane solution tends to be vertical, while the other two are horizontal. At greater depths, where the principal stress axes can assume a more general orientation, the alignment of P , T , and B axes would also tend to assume a more general orientation. We char-

acterize this tendency by inspecting the distribution of plunge angles of P , T , and B axes. We also inspect the magnitude of the components of the moment tensor M_{xz} and M_{yz} as a function of depth for seismicity in northern California and find that it is low at the surface, reaches a peak at depths corresponding to depths of greatest microearthquake activity, and then decreases again as the lower boundary of the seismogenic zone is approached. We interpret this depth variation as being due to the nature of the stress field: Near the surface its axes orientations are constrained to be vertical and horizontal, but at depth they may vary. In this paper we show observations that suggest an alignment near the base of the seismogenic zone, which may arise from a weak horizontal layer in the deeper crust.

2. Focal Mechanism Data

We consider seismic events between 1968 and May 1999 in northern California that were recorded by the Northern California Seismic Network. Out of a total of 58,884 events, we use 32,426 that are within the greater San Andreas fault system (Figure 1b). Within the box in Figure 1b the data sample different structural regions

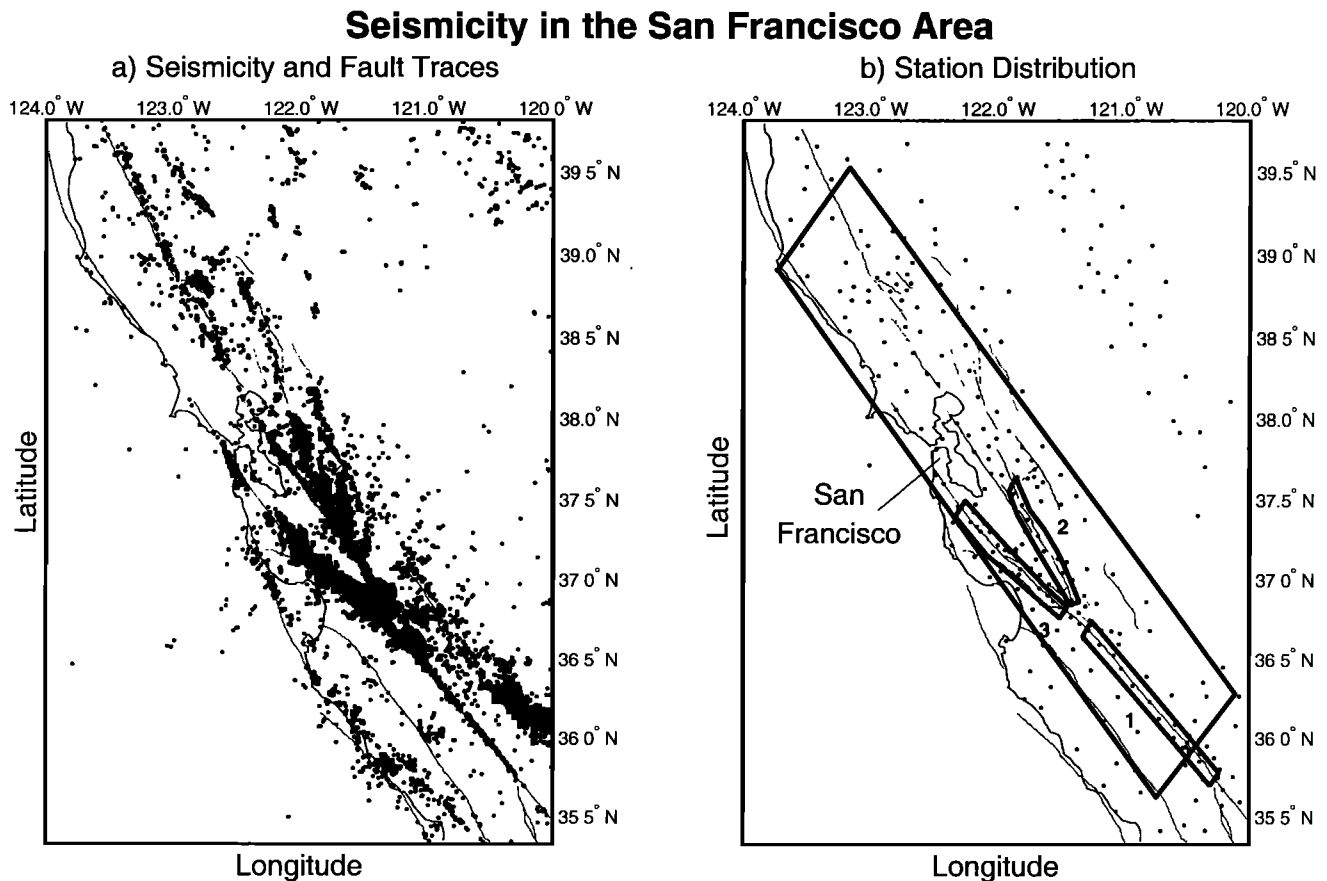


Figure 1. (a) Earthquakes and fault traces in northern California. (b) Distribution of seismic stations in relation to the fault traces. Events selected for this study are within the large box, which was selected based on seismic station density. Also shown are (1) the creeping section, (2) the Loma Prieta Segment of the San Andreas Fault and (3) the Calaveras Fault.

and several major fault zones. In this paper we focus on general properties of the area in the box. However, we also consider three of the most seismogenic fault zone regions in the area individually (Figure 1b): two segments of the San Andreas Fault (creeping section and the Loma Prieta segment) and also the part of the Calaveras Fault, which has failed in a series of moderate earthquakes during the period and was therefore quite active.

Focal mechanisms as well as earthquake locations were determined using a set of local velocity models to best accommodate the laterally varying structure [Oppenheimer *et al.*, 1993]. From the subset of 32,426 events we select focal mechanisms if they satisfy a set of quality criteria, which pertain primarily to formal errors of faultplane orientation and event location, but also to the data set of first-motion observations and to parameters arising during focal mechanism inversion and source location determination. These are specifically: (standard) error of strike $< 40^\circ$; error of dip $< 40^\circ$; error of rake $< 40^\circ$; root-mean-square (RMS) travel time residual ≤ 0.25 s; horizontal location error ≤ 2 km; vertical location error ≤ 2 km; number of first-motion observations ≥ 24 ; maximum azimuthal gap $\leq 90^\circ$; ratio of automatic/human picks ≤ 0.4 ; quality of station distribution ≥ 0.3 ; focal mechanism solution misfit ≤ 0.4 ; convergence parameter = 0; multiple solutions parameter = 0. The parameters and the programs used for determining focal mechanism solutions from the first-motion observations are described by Reasenberg and Oppenheimer [1985]. In this study the threshold values were chosen visually to eliminate the tails of the distribution. These steps reduce the number of events from 32,426 to 11,326. We also excluded explosions from the data set. Since underconstrained events generally violate several of the above criteria, the resulting data set is similar to one obtained from criteria of previous studies [Reasenberg and Oppenheimer, 1985; Amelung and King, 1997]. We impose no limit on source depth (or magnitude) in this study. Unreliable small events are eliminated by other criteria. The first aspect of this data set that we examine is the orientation of earthquake focal mechanisms near Earth's surface.

3. Stress Orientation, the Free Surface, and Focal Mechanism Orientation

At a free surface, across which no shear stresses are transferred, we have

$$\sigma_{xz} = \sigma_{yz} = 0 \quad (1)$$

with the z axis (vertical) perpendicular to the surface. From the eigenvalue problem,

$$(\sigma^0 - \lambda)\mathbf{x} = 0 \quad (2)$$

with

$$\sigma^0 = \begin{pmatrix} \sigma_{xx} & \sigma_{xy} & 0 \\ \sigma_{xy} & \sigma_{yy} & 0 \\ 0 & 0 & \sigma_{zz} \end{pmatrix}, \quad (3)$$

we see that one eigenvector (principal stress axis) is vertical and hence the other two must be horizontal. The orientation of the stress field at Earth's surface has long been used to interpret fault orientation (e.g., Anderson, 1951]. At larger depths the orientation of the stress may or may not align with the free surface. Note, that (1) does not constrain the distance range from the free surface over which the axes orientations are aligned.

The orientation of focal mechanisms, in particular, the pressure, null, and tension (P , T , and B) axes, place constraints on the orientation and relative magnitude of the principal axes of the stress tensor [McKenzie, 1969]. Many techniques have been developed to infer these properties of the stress tensor from focal mechanism data [Gephart and Forsyth, 1984; Angelier, 1984; Michael, 1984].

Instead of estimating the stress field from the P , T , and B axes, we use the known plunge angles of the principal stress axes near the surface (0° or 90°) to inspect the relation with the P , T , and B axes directly. Figure 2 shows the plunge angles for the P , T , and B axes. Note that these axes align near Earth's surface too (topmost panel), which is most apparent closest to the surface (shallower than 1.5 km). B axes show predominantly vertical alignment (90°), while P and T axes show predominant horizontal alignment (strike-slip) with smaller amounts of thrust and normal faulting events (visually enhanced by the normalization). For larger depths the peaks around the horizontal broaden substantially for both P and T . Figure 2b gives the same display except for the strike-slip events only.

The observed alignment of P and T axes near the surface suggests that as observed in the plunge angles, the focal mechanism orientation reflects the orientation of the principal stress axes. Figure 2 also gives the median plunge error (Appendix A) for the respective depth interval. This error is between 22° and 33° in all depth intervals. These errors are nearly constant but slightly smaller for the shallowest and largest depths. Note that near the surface the distribution width is comparable to this error, indicating that variations between focal mechanisms and stress field orientation could be explained by attributing them to the focal mechanisms alone.

A correspondence between the stress axes and the average P , T , and B axes has been suggested before [e.g., Zoback and Zoback, 1980; Sbar, 1982; Xu *et al.*, 1992], but our observations are different in that we consider the plunge angles only. If the strike angles showed the same behavior, i.e., an alignment of the maximum and minimum compressive stress axes with the P and T axes of the focal mechanism, this would indicate that the fault planes were weak (45° between fault plane and maximum compression stress). For our study area most of the earthquakes have strike-slip focal mechanisms. Thus the distributions of the plunge of the P , T , and B axes for most of the events cannot be used to constrain the relative weakness, or strength, of faults. If

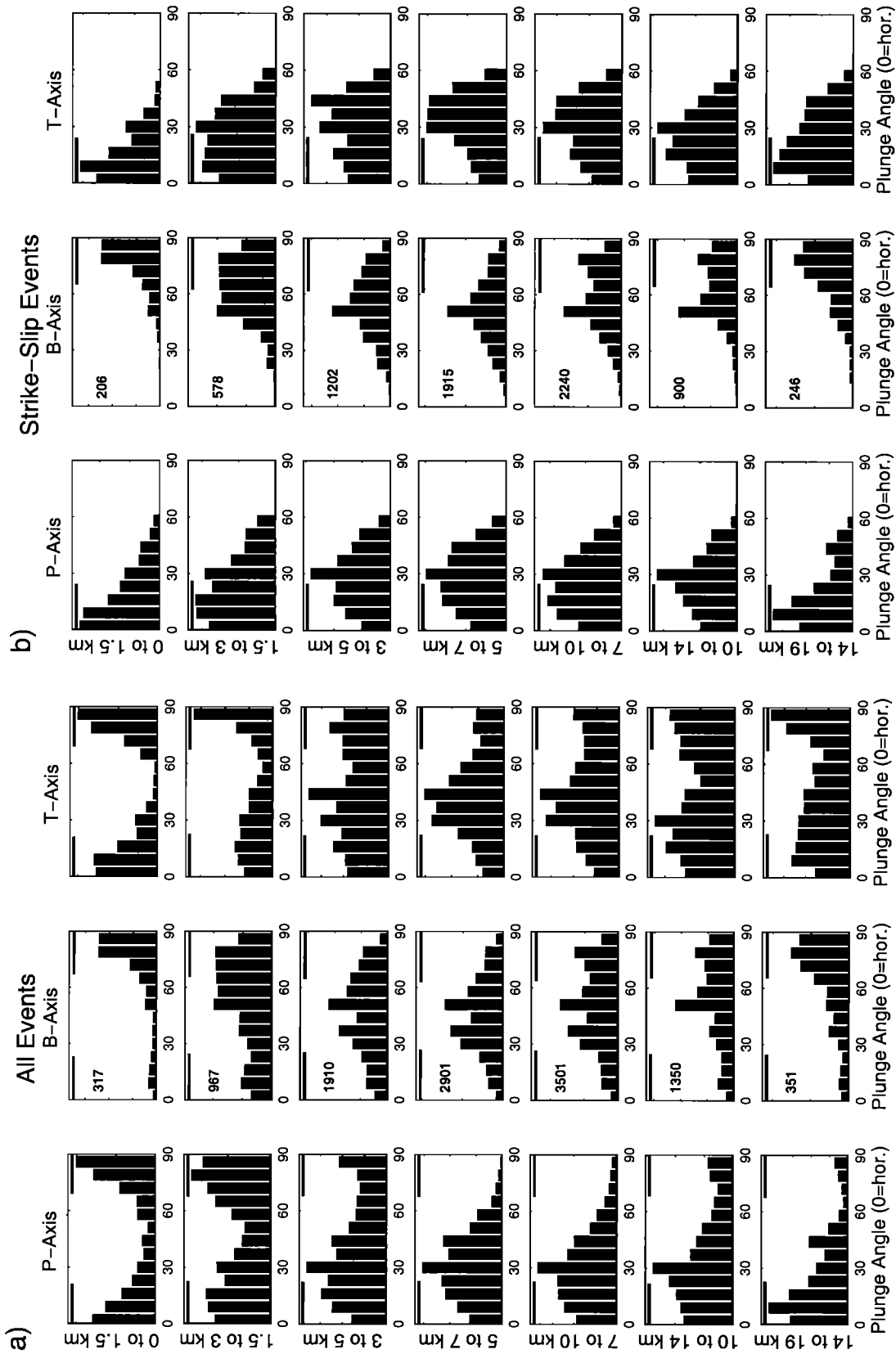


Figure 2. Test of focal mechanism data set from Figure 1 using the expected near-surface effect for all events and (b) for strike-slip events only. For a set of depth intervals, plunge angles of P , B , and T axes are shown (measured from the horizontal). The histograms are normalized by $\cos(\text{plunge})$ to show the correct surface density on the focal sphere. Note the strong alignment near the surface with either the vertical (B axes) or the horizontal direction (P and T axes; see text). Bold numbers indicate the number of events in each depth window. Bars in each panel show the median plunge error (see Appendix A).

the plunge angles reflect the plunge angles of the stress field, they may, however, place constraints on the relative amount of shear traction resolved across a horizontal plane as a function of depth. We use a simple measure of the degree to which each of the P , T , and B axes of the focal mechanism align either vertically or horizontally, as we observe near Earth's surface and use it to track possible variations in focal mechanism alignment as a function of depth.

We characterize the depth variation of focal mechanism orientation using the moment tensor representation. An individual focal mechanism can be represented using a double-couple moment tensor

$$M_{ij} = M_0(\hat{u}_i\hat{n}_j + \hat{u}_j\hat{n}_i) \quad (4)$$

with slip direction \hat{u} , fault plane normal \hat{n} , and scalar seismic moment M_0 . The eigenvectors of the moment tensor are M_0 , 0, and $-M_0$.

We will focus in the following on the relative partitioning of moment onto individual elements of M_{ij} . Therefore we consider normalized moment tensors

$$\bar{M}_{ij} = \frac{1}{\sqrt{2}}(\hat{u}_i\hat{n}_j + \hat{u}_j\hat{n}_i), \quad (5)$$

which have unit Euclidian norm

$$\|\bar{M}_{ij}\|^2 = \bar{M}_{ij} : \bar{M}_{ij} = 1. \quad (6)$$

To quantify the alignment of focal mechanisms, we calculate the quantity

$$m_s = \sqrt{\bar{M}_{xz}^2 + \bar{M}_{yz}^2} \quad (7)$$

and display it as a function of depth. This is motivated by the fact that if these two quantities are zero, the focal mechanism axes are aligned with the horizontal and vertical. Moreover, the corresponding element $t_s = |\mathbf{t}_s| = \sqrt{\sigma_{xz}^2 + \sigma_{yz}^2}$ of the stress tensor represents the shear traction acting on a horizontal plane. In the case of an alignment of stress field and focal mechanism axes we may regard m_s as a proxy for t_s , in a qualitative sense. In particular, if the shear traction is small (e.g., near a traction-free surface), m_s will also show small values. We show in Appendices B and C that aligning the axes of \mathbf{M} and σ follows from maximizing the dot product of resolved shear traction and slip, $\hat{u} \cdot \mathbf{t}_s$, or equivalently maximizing $\mathbf{M} : \sigma$.

We may regard the depth variation of m_s as an indicator of the vertical change of shear traction resolved across a horizontal plane, though only in a relative sense due to the normalization and the limited information content of \mathbf{M} with respect to σ . Note that we do not account for the orientation of shear traction within the horizontal, only the relative magnitude. By studying plunge angles only and not performing stress inversions, we avoid the complicating effects of lateral variations in the stress regime. We take the median over events in depth intervals of 1 km, which are small enough to resolve differences but large enough to contain sufficient data to extract meaningful results.

4. Results

We expect m_s , our proxy for horizontal shear traction, to have small values near the free surface. Indeed, m_s has its lowest values (40-60% of peak values) at the shallowest depths for the whole data set and for the three subsets individually (Figure 3). It reaches a maximum between 5 and 9 km. At greater depth, there is a decrease for all panels, although not as strong as near the surface (to 55-75% of peak values). It is interesting that the maximum of m_s and the depth of maximum seismicity roughly agree, the largest difference between the two being < 3 km. If we use only the strike-slip events, the results are nearly the same, but the uncertainties are larger due to the smaller number of events.

The 95% confidence region suggests that the decrease toward the top and the bottom is statistically significant. This is also reflected in Figure 4, which shows that the low value attained at the base is unlikely to occur randomly. Out of 1000 randomly chosen subsets of the data none produces values as that low. To test whether the depth dependence of m_s is perhaps influenced by the uneven depth distribution of seismicity, we performed tests by randomly reordering the 19,523 moment tensors while keeping source depths fixed. The resulting m_s shows hardly any depth variations and no coherent depth dependence. Thus we exclude the hypothesis that we might be dealing with an artifact resulting from an uneven data distribution. Instead, the depth dependence results from true changes in the moment tensor orientation with depth. We also test whether we are perhaps seeing the effect of depth-dependent changes in event type.

Our results when viewed separately by event types for the entire data set (Figure 5) show that the region is dominated by strike-slip events with much smaller numbers of thrust and normal faulting events. This suggests that $\gamma = (\sigma_2 - \sigma_3)/(\sigma_1 - \sigma_3) \sim 0.5$. The similar seismicity-depth histograms for each event type supports our interpretation and further suggests that averaged over the entire region, there are no systematic stress field rotations with depth (e.g., from strike slip near the surface to normal faulting at depth) and that the average γ is constant with depth in this region. This contrasts with regions studied by *Vetter and Ryall* [1983] and *Iio* [1996]. These studies found transitions between different event types (strike-slip, normal, or thrust faulting) indicating depth-dependent changes in the stress state. The observed depth variation in both of these studies is attributed to increasing overburden with depth. In contrast, this paper reports depth variation in the degree to which motion on faults is controlled by the stress boundary conditions.

5. Discussion

Near the surface we find a statistically significant decrease in our proxy for horizontal shear traction m_s as expected from the surface boundary condition. This suggests that stresses near the surface are more closely

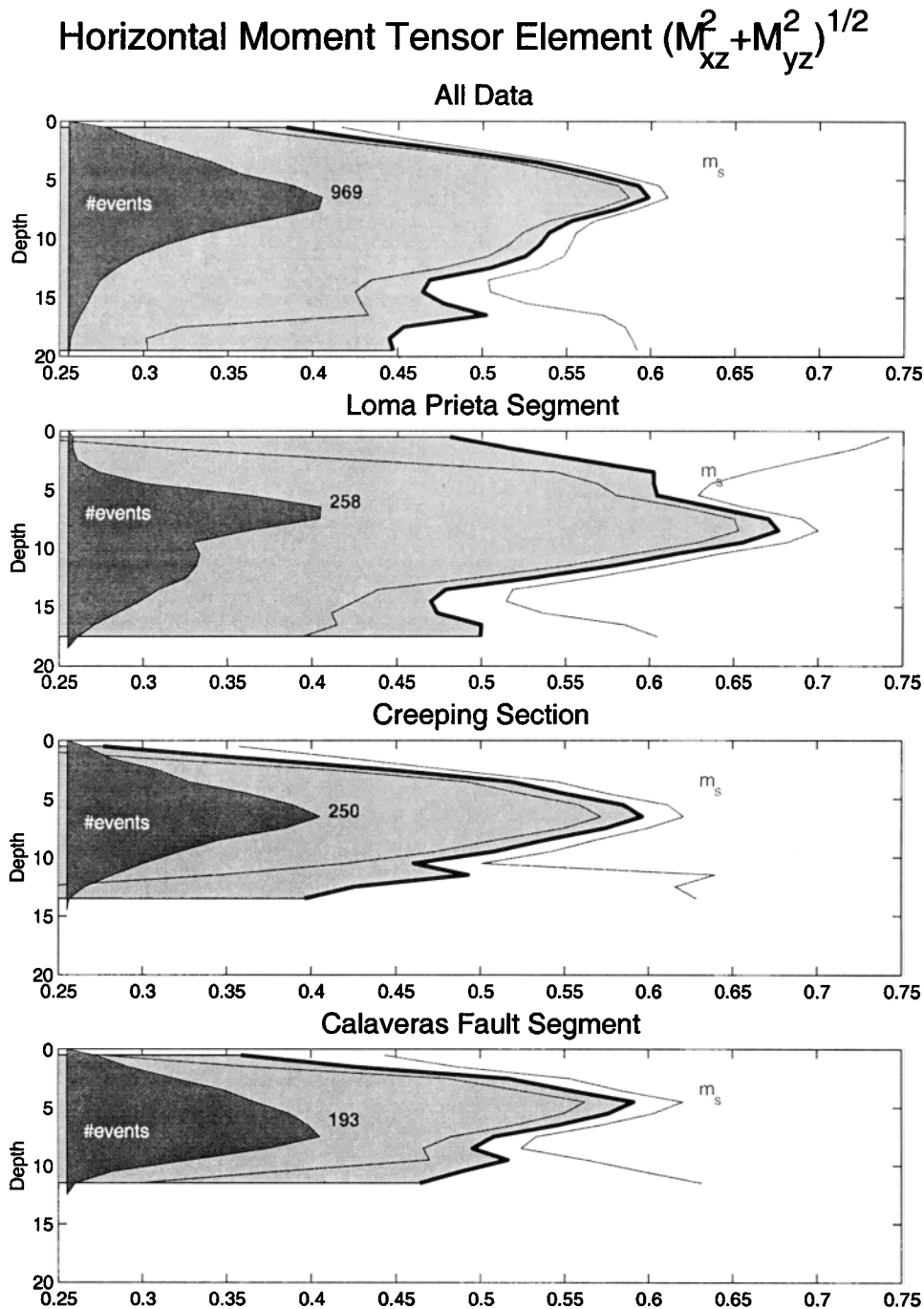


Figure 3. Magnitude of the dimensionless proxy of shear traction on a horizontal plane m_s (equation (7); light shading) at different depths for (a) the entire data set and three subsets essentially covering (b) the Loma Prieta segment of the San Andreas Fault, (c) the creeping section, and (d) a part of the Calaveras Fault (averaged over 1-km intervals, smoothed by three-point running mean). Earthquake frequency as a function of depth is shown in dark shading; numbers give the maximum value. Thin lines give the 95% confidence level of the mean. Note that m_s has its maximum near the depth of maximum earthquake occurrence. There is decreased m_s near the surface and also at larger depth (see text).

aligned to a vertical-horizontal coordinate frame than at larger depths. It is also reflected in the wider distribution of plunge angles of P and T axes in Figure 2 at intermediate depths as compared with the shallowest 3 km. This suggests that the vertical stress may be a

principal stress when averaging over a larger region, but local variations are considerable at intermediate depths in the upper crust (deeper than 3 km). Such local variations out of the vertical are consistent with other studies [McGarr and Gay, 1978]. On the other hand, data from

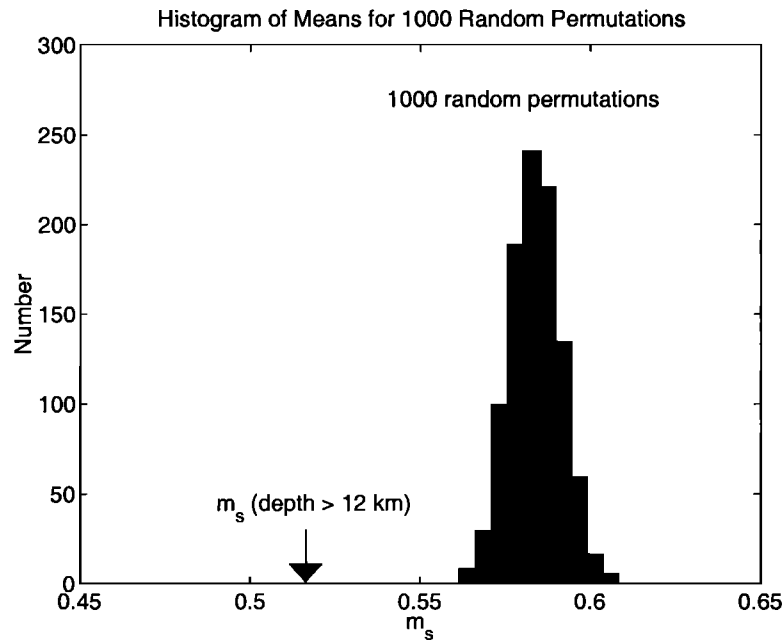


Figure 4. Significance test of low m_s values near the base of the seismogenic crust. The histogram shows m_s values for 1000 random permutations of 785 events (number of events deeper than 12 km) from the entire data set of Figure 3a. None of the realizations was as low as that of the observed m_s , leading to the conclusion that the observed low values of m_s are highly significant.

the German Continental Deep Drilling Program (KTB) borehole in southern Germany suggest that in that region the vertical stress is a principal stress down to 8 km depth [Brudy *et al.*, 1997].

Our observations suggest that the shear traction resolved across horizontal planes reaches a maximum at the depth of maximum seismicity and then decreases toward the base of the seismogenic zone in each of the three subregions. This suggests the presence of another "free surface" near the base of the brittle crust. The distribution of plunge angles of P and T axes is also narrower around the horizontal (Figure 2) at large depths.

Our procedure allows for heterogeneity in the stress field. Namely, the stress field can be laterally heterogeneous. It need only satisfy the stress free boundary condition at the free surface and perhaps a low stress boundary condition at depth. In particular, strike angles may vary substantially from point to point near the surface, while plunge angles must satisfy the boundary conditions. Neither estimation of regional deformation [Kostrov, 1974] nor stress inversion [Gephart and Forsyth, 1984; Angelier, 1984; Michael, 1984] has this property.

However, an alternative explanation for our observations might be a geometrical effect rather than one arising from depth variation in the stress orientation; for example, there might be systematic changes in the orientation of fault planes available for slip to occur on as a function of depth. To address this possibility, Figure 6 considers strike-slip events, for which we can assume that strike is more nearly parallel to the San

Andreas fault system than perpendicular. This provides a basis for distinguishing the slip vector from the fault plane normal vector for individual earthquakes. Figure 6 shows that slip vectors at intermediate depths on average differ from the value at the surface much more than the fault plane normal does. Fault planes are nearly vertical at all depths. This argues against attributing our observations to changes in fault zone geometry. That also appears unlikely since it would require fault zones to become more complex at depth. If anything, fault zones are thought to grow geometrically more complex near Earth's surface, as, for example, in flower structures [Scholz, 1990].

To illustrate the depth change of focal mechanism alignment better, we have made use of an assumed correspondence between plunges of focal mechanism axes and stress field axes also for larger depths as well. This assumption is not critical. Our inferences are valid for the geometry of seismic strain in any case. That leads to the same conclusions regarding the weakness of the deeper layer. Namely, the alignment of slip direction with the horizontal (for strike-slip events) or, equivalently, the lack of oblique slip suggests a weak zone at depth, causing faulting analogous to Andersonian faulting near the surface.

The fact that the slip vector, rather than the fault plane normal vector, appears to be the source of the observed variation also argues against the possibility that lateral refraction effects, which are known to occur along parts of the San Andreas Fault [McNally and McEvilly, 1977] are biasing our results. If these effects

Horizontal Moment Tensor Element $(M_{xz}^2 + M_{yz}^2)^{1/2}$

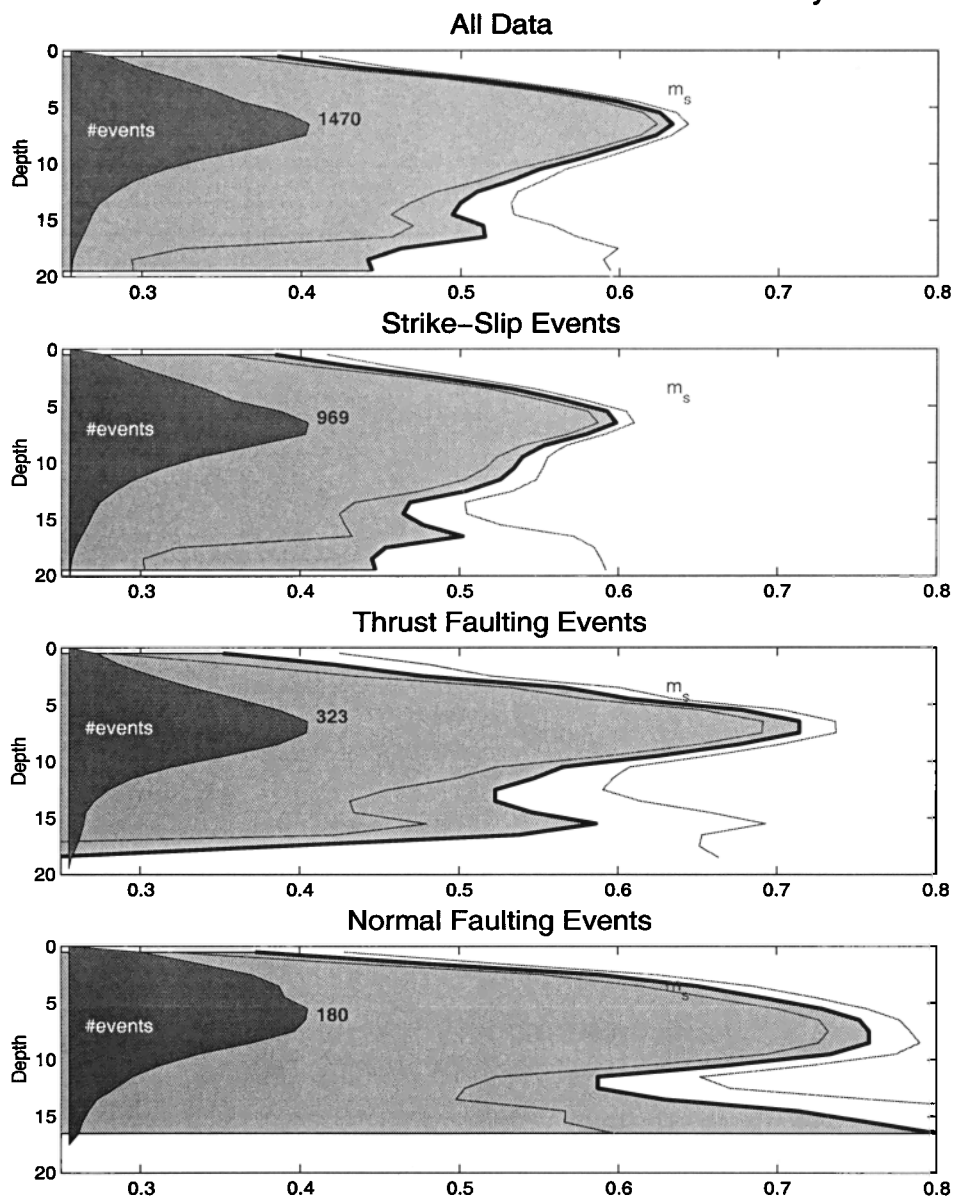


Figure 5. Same as Figure 3 but for different event types in the entire data set (see text).

did exert a strong influence on fault plane solutions, we would expect them to be most prominent for the fault zone parallel nodal plane.

It is interesting to test whether these results depend on individual event types. Figure 5 shows a display similar to Figure 3 for strike-slip, thrust, and normal faulting individually. The dominant strike-slip events produce a pattern similar to the total data set. Results for all three event types show general agreement in that there is a clear decrease from the maximum near 7 km, toward the top and toward the bottom. On the other hand, thrust and normal faulting events show generally larger values than strike-slip events at intermediate depths. This may be due to deviations between the coordinate systems of stress field and moment ten-

sors, which show up for dip-slip events but are less pronounced for strike-slip events since σ_1 and σ_3 are most likely near the P - T -plane. Another interesting feature is that the deepest normal faulting events show an increase rather than a decrease. Closer inspection showed that most of these events were aftershocks of the Loma Prieta events. This may suggest a perturbed stress state in the deeper crust after the Loma Prieta mainshock.

6. Conclusions

Inspecting depth dependences of the orientations of moment tensors has given new insights into the nature of the stress field within the crust. We find that plunge angles of P and T axes of earthquakes in northern Cal-

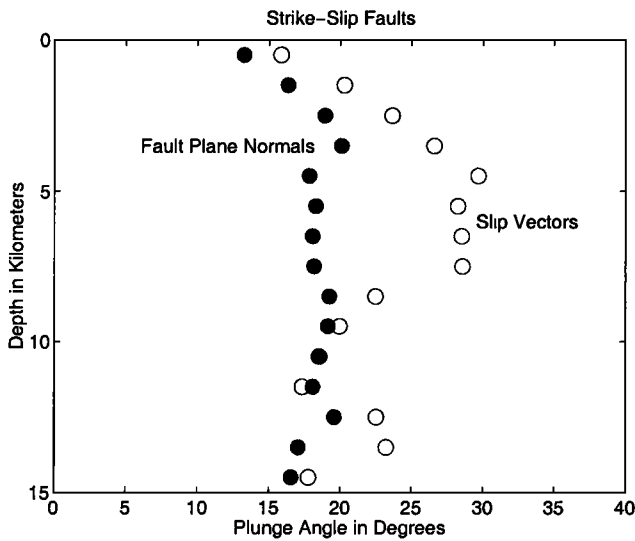


Figure 6. Plunge angles of slip vector and fault plane normals for strike-slip events (assuming strike angles nearly parallel to the dominant faults in the area; range of -45° to 45° and 135° to 225°). Note that fault planes are nearly vertical at all depths, while slip vectors vary with depth, suggesting that it is the stress field rather than fault zone geometry that is changing.

ifornia tend to align in the horizontal plane at shallow depths, suggesting that focal mechanism data are reliable and that their plunge angles can be used to study plunge angles of the stress field. Our relative measure of the shear traction acting on horizontal planes decreases toward the surface, as expected from the surface boundary conditions. We find a similar behavior in the

deeper levels of the seismogenic crust too. This (and an alternative interpretation based on strain) suggests the presence of a weak lower crust, which may partly decouple upper crust and mantle. Figure 7 shows our interpretation of the observations. While the alignment near the surface persists for all times, the alignment near the base of the seismogenic crust is time-dependent due to stress relaxation and stress transfer to and from the lower crust. Our observations cover the interval 62-93 years after the 1906 earthquake, which was the last major earthquake in the area. Orientations near the upper/lower crust boundary are apparently approaching the aligned orientation that we would expect if that boundary were a low-traction surface. This suggests that lower crustal relaxation times are shorter than our observation interval. That is in agreement with viscosity estimates of the order of 10^{18} Pa-s from postseismic deformation following the Northridge and Landers earthquakes [Deng *et al.*, 1998, 1999; Kenner and Segall, 2000]. A unique strength of our technique, however, is its depth resolution: The low-viscosity zone appears to be within the lower crust, rather than below it.

Stress relaxation in the lower crust suggests that secular forces, which act on the upper crust and which ultimately cause earthquakes, are transmitted mainly through the crust (from the side) rather than from the underlying mantle, at least in the vicinity of fault zones. This may indicate that on plate boundary scales, crustal blocks do not simply follow the mantle flow as suggested by England and Jackson [1989] and Bourne *et al.* [1998] and that the style of mantle deformation in these zones is not necessarily coherent with crustal deformation. On

Stress Field as a Function of Time (schematic)

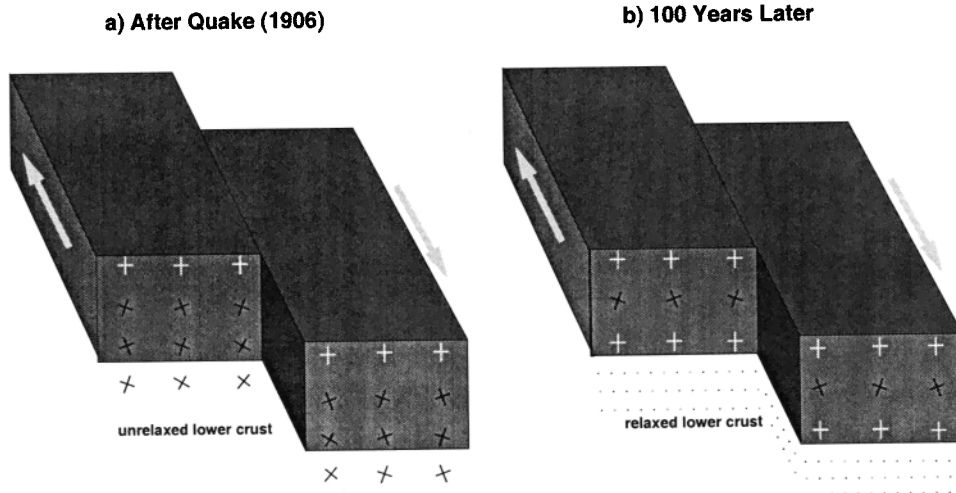


Figure 7. Schematic illustration of the stress field geometry in the crust near a strike-slip fault (a) after quake and (b) 100 years later. For simplicity, only two of the three principal stress axes are shown (black; white where aligned by a traction-free surface). The stress field near the surface has vertical and horizontal principal axes (0 or 90° plunges). Strike angles are not constrained by the free surface and therefore are not shown here. The stress field orientation in deeper parts of the upper (seismogenic) crust (boxes) and the lower crust is time-dependent due to stress transfer after major earthquakes (Figure 7a). Lower crustal stresses relax with time. The upper/lower crustal transition approaches a low-traction surface (Figure 7b, see text).

the contrary, this decoupling might allow separate motion of upper crust and mantle lithosphere. In particular, it might allow block rotation of small upper crustal blocks near major faults in response to the driving acting from the side with decoupling below.

It would be interesting to see how stress fields in other regions behave and how widespread a weak lower crust is in the crust/lithosphere system. The part of the Pacific-North America plate boundary that we have studied is particularly simple since it is predominantly transcurrent. In other places, such as southern California, where the tectonic regime is more complex with significant convergence and vertical deformation, the picture may not be so simple. It would also be interesting to look for signs of time-dependent stress orientation in the lowermost part of the seismogenic crust following large earthquakes as the inferred low strength zone relaxed. Understanding the behavior of the lower crust is particularly important since many large earthquakes nucleate near the upper/lower crustal boundary.

In principle, the technique that we have outlined may provide a means of constraining the nature and rate of transmission of stress between the elastic-brittle regime at seismogenic depths with the more ductile substrate below it. This approach may yield new bounds on lower crustal relaxation times in the vicinity of active fault zones.

Appendix A: Error of Axis Plunge

In this appendix we determine errors of the orientations \hat{P} , \hat{B} , and \hat{T} of the P , T , and B axes, which result from errors of focal mechanism parameters, namely, errors in strike, plunge, and rake angles.

The transformation between fault plane coordinates \mathbf{x}' and spatial coordinates \mathbf{x} can be performed using the

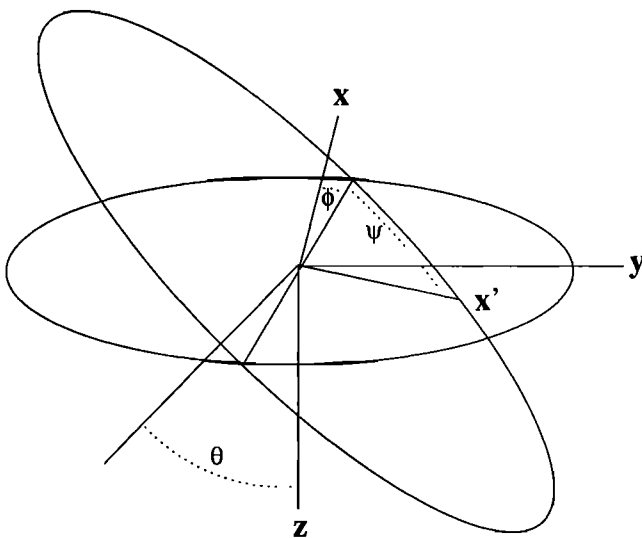


Figure A1. Illustration of the transformation between focal mechanism axes (x' , y' , z') and spatial coordinates (x , y , z).

three Euler angles ϕ , θ , and ψ [Goldstein, 1959] (see Figure A1). The seismological convention is related to these angles as strike angle ϕ , plunge angle θ , and rake angle $-\psi$.

To describe the orientations of fault plane coordinates in spatial coordinates, we need the inverse transformation matrix \mathbf{R} :

$$\mathbf{R} = \begin{pmatrix} \cos \psi \cos \phi - \cos \theta \sin \phi \sin \psi & & \\ \cos \psi \sin \phi + \cos \theta \cos \phi \sin \psi & & \\ \sin \theta \sin \psi & & \\ -\sin \psi \cos \phi - \cos \theta \sin \phi \cos \psi & \sin \theta \sin \phi & \\ -\sin \psi \sin \phi + \cos \theta \cos \phi \cos \psi & -\sin \theta \cos \phi & \\ \sin \theta \cos \psi & \cos \theta & \end{pmatrix}, \quad (\text{A1})$$

which operates as $\mathbf{x} = \mathbf{R}\mathbf{x}'$. Thus the columns of \mathbf{R} give the orientations of the axes $\hat{\mathbf{x}}'$, $\hat{\mathbf{y}}'$, and $\hat{\mathbf{z}}'$. If $\hat{\mathbf{x}}'$ is the direction of slip, then the B axis, which is within the fault and perpendicular to $\hat{\mathbf{x}}'$, has orientation

$$\hat{\mathbf{B}} = \begin{pmatrix} -\sin \psi \cos \phi - \cos \theta \sin \phi \cos \psi \\ -\sin \psi \sin \phi + \cos \theta \cos \phi \cos \psi \\ \sin \theta \sin \psi \end{pmatrix} \quad (\text{A2})$$

$\hat{\mathbf{T}}$, the orientation of the tension axis, is halfway between $\hat{\mathbf{x}}'$ and $\hat{\mathbf{z}}'$

$$\hat{\mathbf{T}} = \frac{1}{\sqrt{2}} \begin{pmatrix} \cos \psi \cos \phi - \cos \theta \sin \phi \sin \psi + \sin \theta \sin \phi \\ \cos \psi \sin \phi + \cos \theta \cos \phi \sin \psi - \sin \theta \cos \phi \\ \sin \theta \sin \psi + \cos \theta \end{pmatrix}, \quad (\text{A3})$$

and $\hat{\mathbf{P}}$, the orientation of the compression direction, is

$$\hat{\mathbf{P}} = \frac{1}{\sqrt{2}} \begin{pmatrix} \cos \psi \cos \phi - \cos \theta \sin \phi \sin \psi - \sin \theta \sin \phi \\ \cos \psi \sin \phi + \cos \theta \cos \phi \sin \psi + \sin \theta \cos \phi \\ \sin \theta \sin \psi + \cos \theta \end{pmatrix}. \quad (\text{A4})$$

From these we calculate the errors of plunge angle depending on errors in the fault-plane orientation. Since the plunge of an axis is $\text{asin}(z)$ with the vertical component z , its error is

$$\frac{1}{\sqrt{1-z^2}} \sqrt{\left(\frac{\partial z}{\partial \theta}\right)^2 d^2 \theta + \left(\frac{\partial z}{\partial \psi}\right)^2 d^2 \psi}.$$

The partial derivatives are given in Table 1. As one may expect, the plunge error does not depend on the error of strike.

Appendix B: Alignment of Moment Tensor and Stress Field Axes

Consider the force acting on a horizontal plane, normal to the vertical $\hat{\mathbf{z}}$ [e.g., Aki and Richards, 1980]. This force, the traction vector, is

$$\mathbf{t} = \sigma \cdot \hat{\mathbf{z}} = \sigma_{xz} \hat{\mathbf{x}} + \sigma_{yz} \hat{\mathbf{y}} + \sigma_{zz} \hat{\mathbf{z}}. \quad (\text{B1})$$

We assume that fault friction is isotropic such that slip occurs in the direction of maximum resolved shear traction [McKenzie, 1969]. The orientation of the slip vector $\hat{\mathbf{u}}$ will maximize the quantity

Table 1. Partial Derivatives

	<i>B</i>	<i>T</i>	<i>P</i>
$\partial z/\partial\theta$	$\cos\psi\cos\theta$	$\frac{1}{\sqrt{2}}(\sin\psi\cos\theta - \sin\theta)$	$\frac{1}{\sqrt{2}}(\sin\psi\cos\theta + \sin\theta)$
$\partial z/\partial\psi$	$-\sin\theta\sin\psi$	$\frac{1}{\sqrt{2}}\sin\theta\cos\psi$	$\frac{1}{\sqrt{2}}\sin\theta\cos\psi$

$$S = |\hat{\mathbf{u}} \cdot \mathbf{t}_s|, \tag{B2}$$

where the resolved shear traction \mathbf{t}_s is

$$\mathbf{t}_s = \sigma \cdot \hat{\mathbf{n}} - \hat{\mathbf{n}} \cdot (\sigma \cdot \hat{\mathbf{n}})\hat{\mathbf{n}}. \tag{B3}$$

Thus we seek to maximize

$$S = |\hat{\mathbf{u}} \cdot (\sigma \cdot \hat{\mathbf{n}} - \hat{\mathbf{n}} \cdot (\sigma \cdot \hat{\mathbf{n}})\hat{\mathbf{n}})|. \tag{B4}$$

Since $\hat{\mathbf{n}}$ and $\hat{\mathbf{u}}$ are orthogonal, the second term is zero and (B2) is equivalent to

$$S = |\mathbf{M} : \sigma|, \tag{B5}$$

or in indicial notation

$$S = |M_{ij}\sigma_{ij}|. \tag{B6}$$

[Beroza and Zoback, 1993]. Near the free surface, σ_{xz} , σ_{yz} , and σ_{zz} approach zero (equation (2)). Thus, the corresponding components of the moment tensor (M_{xz} , M_{yz} , and M_{zz}) cannot contribute to maximizing $\mathbf{M} : \sigma$. Appendix C shows that (B2) and (B5) are maximized when the axes of \mathbf{M} and σ are aligned. In this case, $M_{xz} = M_{yz} = M_{zz} = 0$. The only difference at the base of the seismogenic zone is that the σ_{zz} component of the stress tensor will not be zero. In this case the same argument holds, except that $\mathbf{M} : \sigma$ will be maximized when only the M_{xz} and M_{yz} components of the moment tensor are zero.

Appendix C: Free Surface and the Moment Tensor

Consider a coordinate system with axes in the directions of the stress axes. At a free surface the z -axis is taken to be vertical. In this coordinate system we have

$$\sigma = \begin{pmatrix} \sigma_1 & 0 & 0 \\ 0 & \sigma_2 & 0 \\ 0 & 0 & \sigma_3 \end{pmatrix} \tag{C1}$$

with the σ_i not necessarily ordered by size. We want to know which constraints a free surface imposes on a moment tensor \mathbf{M}

$$\mathbf{M} = \begin{pmatrix} M_{11} & M_{12} & M_{13} \\ M_{12} & M_{22} & M_{23} \\ M_{13} & M_{23} & M_{33} \end{pmatrix}, \tag{C2}$$

e.g., on its orientation. We do this by relating \mathbf{M} to a moment tensor \mathbf{M}'

$$\mathbf{M}' = \begin{pmatrix} M_0 & 0 & 0 \\ 0 & -M_0 & 0 \\ 0 & 0 & 0 \end{pmatrix}, \tag{C3}$$

which has been chosen to have the same principal axes as the stress field

$$\mathbf{M} = \mathbf{R} \mathbf{M}' \mathbf{R}. \tag{C4}$$

We are looking for maxima of the outer product of moment tensor and stress field (equation (B5))

$$\begin{aligned} E &= M_{ij}\sigma_{ij} = \sigma_1 M_{11} + \sigma_2 M_{22} + \sigma_3 M_{33} \\ &= M_0 \left[(R_{11}^2 - R_{12}^2)\sigma_1 + (R_{12}^2 - R_{22}^2)\sigma_2 + (R_{13}^2 - R_{23}^2)\sigma_3 \right], \end{aligned} \tag{C5}$$

which is

$$\begin{aligned} E &= M_0 \sigma_1 \left[(\cos^2\psi - \sin^2\psi)(\cos^2\phi - \sin^2\phi\cos^2\theta) \right. \\ &\quad \left. - 4 \cos\psi\sin\psi\cos\phi\sin\phi\cos\theta \right] \\ &\quad + M_0 \sigma_2 \left[(\cos^2\phi - \sin^2\phi)(\sin^2\psi - \cos^2\theta\cos^2\psi) \right. \\ &\quad \left. + 4 \cos\theta\sin\psi\cos\psi\sin\phi\cos\phi \right] \\ &\quad + M_0 \sigma_3 \sin^2\theta. \end{aligned} \tag{C6}$$

The partial derivatives of E with respect to θ , ϕ , and ψ are

$$\begin{aligned} \frac{\partial E}{\partial\theta} &= M_0 \sigma_1 \left\{ 2 \sin^2\phi [\sin\theta\cos\theta] (\cos^2\psi - \sin^2\psi) \right. \\ &\quad \left. + 4 [\cos\psi\sin\psi] [\sin\phi\cos\phi] \sin\theta \right\} \\ &\quad + M_0 \sigma_2 \left\{ 2 \cos^2\psi [\sin\theta\cos\theta] (\cos^2\phi - \sin^2\phi) \right. \\ &\quad \left. - 4 [\sin\psi\cos\psi] [\sin\phi\cos\phi] \sin\theta \right\} \\ &\quad + M_0 \sigma_3 \left\{ 2 [\sin\theta\cos\theta] \right\}, \end{aligned} \tag{C7}$$

$$\begin{aligned} \frac{\partial E}{\partial \phi} = M_0 \sigma_1 & \left\{ -2 [\cos \phi \sin \phi] (\cos^2 \psi - \sin^2 \psi) (1 + \cos^2 \theta) \right. \\ & \left. - 4 [\cos \psi \sin \psi] \cos \theta (\cos^2 \phi - \sin^2 \phi) \right\} \\ + M_0 \sigma_2 & \left\{ -3 [\sin \phi \cos \phi] (\sin^2 \psi - \cos^2 \psi \cos^2 \theta) \right. \\ & \left. + 4 \cos \theta [\sin \psi \cos \psi] (\cos^2 \phi - \sin^2 \phi) \right\} \quad (C8) \end{aligned}$$

$$\begin{aligned} \frac{\partial E}{\partial \psi} = M_0 \sigma_1 & \left\{ -4 [\cos \psi \sin \psi] (\cos^2 \phi - \sin^2 \phi \cos^2 \theta) \right. \\ & \left. - 4 [\sin \phi \cos \phi] \cos \theta (\cos^2 \psi - \sin^2 \psi) \right\} \\ + M_0 \sigma_2 & \left\{ 2 [\cos \psi \cos \psi] (1 + \cos^2 \theta) (\cos^2 \phi - \sin^2 \phi) \right. \\ & \left. + 4 [\sin \phi \cos \phi] \cos \theta (\cos^2 \psi - \sin^2 \psi) \right\}. \quad (C9) \end{aligned}$$

The combination of sine and cosine terms in brackets show that a solution of $\partial E/\partial \theta = \partial E/\partial \phi = \partial E/\partial \psi = 0$ is obtained if all of θ , ϕ , and ψ take values of 0, $\pi/2$, π , or $3\pi/2$. Therefore extreme values of E occur if the principal axes of \mathbf{M} are parallel to those of the stress tensor σ .

Note that this is the case for any surface which cannot support shear tractions. The free surface, which also has $\sigma_{zz} = 0$, is a special case of this.

Acknowledgments. We thank the Northern California Earthquake Data Center for providing catalog and waveform data. Important discussion with Norman Sleep, Mark Zoback, Bill Ellsworth, Jean Chery, Andy Michael, and David Oppenheimer are acknowledged. David Oppenheimer also supplied us with focal mechanism inversion software. We also want to thank Mike Gurnis, Roger Buck and an anonymous reviewer for thoughtful comments in the review process. G.H.B. is supported by a Heisenberg-Fellowship of the Deutsche Forschungsgemeinschaft.

References

- Aki, K., and P.G. Richards, *Quantitative Seismology, Theory and Methods*, vol. I, W.H. Freeman, New York, 1980.
- Amelung, F., and G. King, Large-scale tectonic deformation inferred from small earthquakes, *Nature*, *386*, 702-705, 1997.
- Anderson, E.M., *The Dynamics of Faulting*, Oliver and Boyd, White Plains, N.Y., 1951.
- Angelier, J., Tectonic analysis of fault slip data sets, *J. Geophys. Res.*, *89*, 5835-5848, 1984.
- Beroza, G.C., and M.D. Zoback, Mechanism diversity of the Loma Prieta aftershocks and the mechanics of mainshock-aftershock interaction, *Science*, *259*, 210-213, 1993.
- Bourne, S.J., P.C. England, and B. Parsons, The motion of crustal blocks driven by flow of the lower lithosphere and implications for slip rates of continental strike-slip faults, *Nature*, *391*, 655-659, 1998.
- Brudy, M., M.D. Zoback, K. Fuchs, F. Rummel, and J. Baumgärtner, Estimation of the complete stress tensor to 8 km in the KTB scientific drill holes: Implications for crustal strength, *J. Geophys. Res.*, *102*, 18,453-18,475, 1997.
- Deng, J., M. Gurnis, H. Kanamori, and E. Hauksson, Viscoelastic flow in the lower crust after the 1992 Landers, California, earthquake, *Science*, *282*, 1689-1692, 1998.
- Deng, J., K. Hudnut, M. Gurnis, and E. Hauksson, Stress loading from viscous flow in the lower crust and triggering of aftershocks following the 1994 Northridge, California, earthquake, *Geophys. Res. Lett.*, *26*, 3209-3212, 1999.
- England, P., and J. Jackson, Active deformation of the continents, *Annu. Rev. Earth. Planet. Sci.*, *17*, 197-226, 1989.
- Froidevaux, C., Basin and Range large-scale tectonics: Constraints from gravity and reflection seismology, *J. Geophys. Res.*, *91*, 3625-3632, 1986.
- Fuchs, K., K.P. Bonjer, D. Gajewski, E. Lueschen, C. Prodehl, K.-J. Sandmeier, F. Wenzel, and H. Wilhelm, Crustal evolution of the Rhinegraben area, 1, Exploring the lower crust in the Rhinegraben Rift by unified geophysical experiments, *Tectonophysics*, *141*, 261-275, 1987.
- Gephart, J.W., and D.W. Forsyth, An improved method for determining the regional stress tensor using earthquake focal mechanism data: Application to the San Fernando earthquake sequence, *J. Geophys. Res.*, *89*, 9305-9320, 1984.
- Goldstein, H., *Classical Mechanics*, Addison-Wesley-Longman, Reading, Mass., 1959.
- Iio, Y., Depth-dependent change in the focal mechanism of shallow earthquakes: Implications for brittle-plastic transition in a seismogenic region, *J. Geophys. Res.*, *101*, 11,209-11,216, 1996.
- Iio, I., Frictional coefficient on faults in a seismogenic region inferred from earthquake mechanism solutions, *J. Geophys. Res.*, *102*, 5403-5412, 1997.
- Jackson, J., and D. McKenzie, The geometrical evolution of normal fault systems, *J. Struct. Geol.*, *5*, 471-482, 1983.
- Kenner, S.J., and P. Segall, Postseismic deformation following the 1906 San Francisco earthquake, *J. Geophys. Res.*, *105*, 13,195-13,209, 2000.
- Kostrov, V. V., Seismic moment and energy of earthquakes, and seismic flow of rock, *Phys. Solid Earth*, *1*, 13-21, 1974.
- Lachenbruch, A.H., and J.H. Sass, Thermo-mechanical aspects of the San Andreas Fault system, in *Proceedings of the Conference on Tectonic Problems of the San Andreas Fault System*, pp. 192-205, Stanford Univ. Press, Stanford, Calif., 1973.
- McGarr, A., and N.C. Gay, State of stress in the Earth's crust, *Annu. Rev. Earth Planet. Sci.*, *6*, 405-436, 1978.
- McKenzie, D.P., The relation between fault plane solutions for earthquakes and the directions of the principal stresses, *Bull. Seismol. Soc. Am.*, *59*, 591-601, 1969.
- McNally, K.C., and T.V. McEvilly, Velocity contrast across the San Andreas Fault in central California: Small-scale variations from P-wave nodal plane distortion, *Bull. Seismol. Soc. Am.*, *67*, 1565-1576, 1977.
- Michael, A. J., Determination of stress from slip data: Faults and folds, *J. Geophys. Res.*, *89*, 11,517-11,526, 1984.
- Molnar, P., Brace-Goetze strength profiles, the partitioning of strike-slip and thrust faulting at zones of oblique convergence, and the stress-heat flow paradox of the San Andreas Fault, in *Fault Mechanics and Transport Properties of Rocks, a Festschrift in Honor of W. F. Brace*, edited by B. Evans, pp. 435-459, Academic, San Diego, Calif., 1992.

- Oppenheimer, D.H., P.A. Reasenberg, and R.W. Simpson, Fault plane solutions for the 1984 Morgan Hill, California, earthquake sequence: Evidence for the state of stress on the Calaveras Fault, *J. Geophys. Res.*, *93*, 9007-9026, 1988.
- Oppenheimer, D., F. Klein, J. Eaton, and F. Lester, The northern Californian seismic network bulletin, January-December 1992, *U.S. Geol. Surv. Open File Rep.*, *93-578*, 1993.
- Reasenberg, P.A., D.H. Oppenheimer, FPFIT, FPPLOT and FPPAGE; Fortran computer programs for calculating and displaying earthquake fault-plane solutions, *U.S. Geol. Surv. Open File Rep.*, *85-739*, 1985.
- Royden, L., Coupling and decoupling of crust and mantle in convergent orogens: Implications for strain partitioning in the crust, *J. Geophys. Res.*, *101*, 17,679-17,705, 1996.
- Sbar, M.L., Delineation and interpretation of seismotectonic domains in western North America, *J. Geophys. Res.*, *87*, 3919-3928, 1982.
- Scholz, C.H., The brittle-plastic transition and the depth of seismic faulting, *Geol. Rundsch.*, *77*, 319-328, 1988.
- Scholz, C.H., *The Mechanics of Earthquakes and Faulting*, Cambridge Univ. Press, New York, 1990.
- Shelton, G.L., J. Tullis, and T. Tullis, Experimental high temperature and high pressure faults, *Geophys. Res. Lett.*, *8*, 55-58, 1981.
- Silver, P.G., Seismic anisotropy beneath the continents: Probing the depths of geology, *Annu. Rev. Earth Planet. Sci.*, *24*, 385-432, 1996.
- Thatcher, W., and P. England, Ductile shear zones beneath strike-slip faults; Implications for the thermomechanics of the San Andreas fault zone, *J. Geophys. Res.*, *103*, 891-905, 1998.
- Vetter, U.R., and A. S. Ryall, Systematic changes of focal mechanism with depth in the Western Great Basin, *J. Geophys. Res.*, *88*, 8237-8250, 1983.
- Xu, Z., S. Wang, Y. Huang, and A. Gao, Tectonic stress field of China inferred from a large number of small earthquakes, *J. Geophys. Res.*, *97*, 11,867-11,877, 1992.
- Zoback, M.D., et al., New evidence on the state of stress of the San Andreas fault system, *Science*, *238*, 1105-1111, 1987.
- Zoback, M. L., and M.D. Zoback, State of stress in the conterminous United States, *J. Geophys. Res.*, *85*, 6113-6156, 1980.
- Zuber, M.T., E.M. Parmentier, and R.C. Fletcher, Extension of continental lithosphere: A model for two scales of Basin and Range deformation, *J. Geophys. Res.*, *91*, 4826-4838, 1986.

G.C. Beroza and G. H. R. Bokelmann, Department of Geophysics, Stanford University, Stanford, CA 94305-2215. (goetz@pangea.stanford.edu)

(Received December 13, 1999; revised April 13, 2000; accepted June 5, 2000.)